ELSEVIER

Journal of Contaminant Hydrology 28 (1997) 247–266

JOURNAL OF
Contaminant
Hydrology

Triple-porosity analysis of solute transport

M. Bai [*,1], J.-C. Roegiers

School of Petroleum and Geological Engineering, The University of Oklahoma, Norman, OK, 73019-0628, USA

Received 17 October 1995; revised 12 August 1996; accepted 23 September 1996

Abstract

As an extension to the traditional dual-porosity approach, a triple-porosity model is presented to study the solute transport in heterogeneous porous media where the transport processes are distinctly different between macropores, mesopores and micropores. The distinctions in terms of conductance and storage in the respective pore domain are characterized by the fact that: (a) macropores are primary flow paths where both dispersion and convection are prevalent; (b) mesopores are intermediate flow paths where convection becomes dominant and (c) micropores are supplemental flow paths and mass storage spaces where only diffusive flow is manifested. In cascading coupling, the solute interchange between micropores and mesopores is maintained by assuming micropore diffusion as internal sources (sinks) attached to mesopore skins. A comprehensive solute exchange between macropores and mesopores is preserved. A mathematical model is constructed in accordance with the physical conceptualization. The coupled partial differential equations are solved in a one-dimensional geometry using Laplace transform, and the subsequent coupled ordinary differential equations are circumvented via the method of differential operators. Semi-analytical solutions are obtained. © 1997 Elsevier Science B.V.

Keywords: Solute transport; Triple-porosity; Analytical modeling

1. Introduction

Solute transport through heterogeneous porous media has attracted increased interest owing to the recognized fact that the contaminant plume development under such scenarios cannot be correctly predicted using the conventional theory of flow and transport through a homogeneous medium. The introduced heterogeneities are frequently recorded as ''abnormalities'' such as nonequilibrium changes, abrupt occurrence and

* Corresponding author.
[1] Present address: Rock Mechanics Institute, The University of Oklahoma, OK, USA.

PII S0169-7722(96)00086-1

extensive tailing in solute breakthrough. These phenomena are traditionally interpreted as owing to either one or a combination of the following mechanisms: (a) local flow rectification owing to fluid transport between mobile (flowing) and immobile (dead-end pore) regions (Coats and Smith, 1964); (b) tortuous flow pathways as a result of heterogeneous grain and pore distributions (Bear, 1972); (c) variable flow channels owing to particle–pore clogging, size exclusion and deposition (Joy and Kouwen, 1991; Imdakm and Sahimi, 1991); (d) pollutant directional migration and spatial storage as a consequence of dominant anisotropism in permeability and variation in porosity distributions (Noltimier, 1971; Sardin et al., 1991); (e) regional perturbation of solute concentration owing to velocity contrast between layered and fractured media (McKibbin, 1985; Houseworth, 1988), and (f) fluids and/or formation nonlinear characteristics (Bai and Roegiers, 1994).

It is impractical to consider all above-mentioned factors when studying heterogeneous influences. Owing to the striking resemblance in the resulting solute transport, the research interest appears to focus on one of these influential factors, such as on the impact of two region flow (factor (a)). To address this particular mechanism, Coats and Smith (1964) provided an adequate phenomenological model in which the solute migration in the mobile region was modified by a "quasi-steady" flow between macropores and dead-end pores, useful for characterizing the medium heterogeneities. Using the average-volume theory, Piquemal (1992) derived a slightly different formulation, envisioning the similar scale for the selection of parameters. Coats and Smith's model has been further improved by Bai and Elsworth (1995) through coupling the complete transport processes (dispersion and convection) within so-called "dead-end" pores.

The difference between fluid flow and solute transport can be summarized as that the transported medium is a type of fluid for the former case, but a component of the fluid for the latter scenario (Bear, 1993). Aside from this difference, Coats and Smith (1964)'s model is similar if not identical to the model of Warren and Root (1963) which was primarily used to interpret fluid flow through fractured porous media. In many cases, Coats and Smith's model has received wide references in the modeling of fluid flow and contaminant transport through fractured porous media (Tang et al., 1981; Bibby, 1981; Huyakorn et al., 1983; Nilson and Lie, 1990; Rowe and Booker, 1990; Sudicky and Mclaren, 1992; Harrison et al., 1992; Leo and Booker, 1993). In contrast, however, Warren and Root's model has been rarely mentioned in the literature of solute transport through micropore–macropore regions (Passioura, 1971; Passioura and Rose, 1971; Joy and Kouwen, 1991; Koenders and Williams, 1992; Joy et al., 1993; Piquemal, 1992, Piquemal, 1993) with an exception that Sahimi (1993) provided an implicit link between the two models. As a result of ineffective communication, it appears that the models based on the same conceptualization may have been developed independently (e.g. spherical block model for transport through fractured porous media by Huyakorn et al. (1983), and for transport through micropore–macropore region by Correa et al., 1987). The communication needs to be improved to accelerate the information dissemination between the two seemingly "different" fields.

Owing to the existence of physical and mathematical analogies in modeling flow and transport through fractured porous media and through micropore–macropore media, the

multiporosity/multipermeability model proposed by Bai et al. (1993) can be made applicable to solute transport through multi-pore regions. Parallel effort has been made recently by Gwo et al. (1995) to discretize the partially saturated heterogeneous media into three regions: (a) micropore, (b) mesopore, and (c) macropore, where the inter-region flow is activated in accordance with the state of fluid saturation. In this paper, a complementary effort has been made to provide an alternative triple-porosity analysis for solute transport through fully saturated heterogeneous porous media where the geometric correlation among micro–meso–macro pore regions is more explicitly expressed.

2. Physical conceptualization

In the theory of contaminant transport through homogeneous porous media, the mechanical dispersion is included in the evaluation of total mass flux of the solute to account for the spreading of the solute owing to variations in the seepage velocity (Shackelford, 1993). On a microscopic level, velocity variations will result owing to the tortuous nature of the flow paths existing in nearly all porous materials. On a macroscopic level, the mechanical dispersion may be caused by the variations in flow rates resulting from heterogeneities over a regional scale. An example is that the fluid flows through the bulk sand medium interrupted by the existence of low permeable clay lenses. In the solute transport, the total mass flux of the species can be attributed to the fluxes owing to convection, diffusion and dispersion. Luxmoore et al. (1990) defined that macropores and micropores are those with equivalent pore diameters (EPD) greater than 1 mm and less than 0.01 mm, respectively. Gwo et al. (1995) further divided the pore structures into three regions by adding a mesopore region with the corresponding EPD between 0.005 mm and 1 mm. From practical aspects, it appears that soils consisting of a continuous distribution of pore sizes can be segregated into macropores, mesopores, and micropores, which is analogous to the particles where their size distribution is classified into sand, silt, and clay (Gwo et al., 1995).

While the EPD may be one of the important factors to determine the transport process in porous media at various scales, the effect of heterogeneities with irregular shapes can be more pronounced, especially at greater depths and for fully saturated media. A triple-porosity medium is conceptualized in Fig. 1. Within the selected representative elementary volume (REV) in an aquifer, mass transport primarily occurs through macropores where both hydrodynamic dispersion and convection can be dominant. Mesopores co-exist within the domain of macropores, where the convective flow is prominent owing to both velocity and permeability contrasts between flow channels and solids. Dominant mesopore convection has been experimentally identified by Houseworth (1988), and by Bouhroum and Bai (1996). Sub-discretizing the mesopore areas into micropore regions is necessary in order to envision the dominant diffusive flow process within micropores. Depending on the relative concentration differences between mesopores and micropores, micro-replenishment may occur in lieu of micro-diffusion (analogy to conventional reverse matrix diffusion; Bai and Roegiers, 1995). This

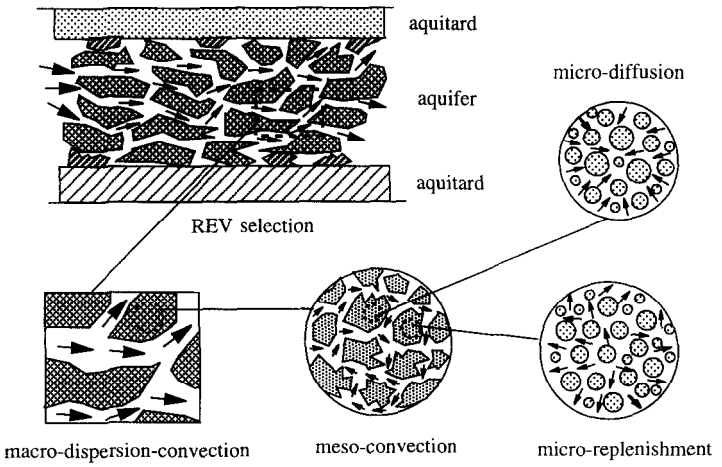

Fig. 1. Schematic triple-porosity scenario.

conceptualization provides a more explicit spatial relationship than the one associated with the multiple-pore-region theory.

3. Mathematical formulation

Assuming constant porosity and using the average velocity v ($v = v^*/n$, v^* is the intrinsic interstitial velocity), also assuming the quasi-steady rate exchange proportional to the concentration gradients between the three continua (Bear, 1972; Bai et al., 1993; Gwo et al., 1995), the general governing equations of solute transport for a triple-porosity system can be described as:

$$\frac{\partial}{\partial x_i}\left(D_{1ij}\frac{\partial c_1}{\partial x_j}\right) - v_{1i}\frac{\partial c_1}{\partial x_i} = \frac{\partial c_1}{\partial t} + \frac{\xi_{12}}{n_1}(c_1 - c_2) + \frac{\xi_{13}}{n_1}(c_1 - c_3) \tag{1}$$

$$\frac{\partial}{\partial x_i}\left(D_{2ij}\frac{\partial c_2}{\partial x_j}\right) - v_{2i}\frac{\partial c_2}{\partial x_i} = \frac{\partial c_2}{\partial t} + \frac{\xi_{21}}{n_2}(c_2 - c_1) + \frac{\xi_{23}}{n_2}(c_2 - c_3) \tag{2}$$

$$\frac{\partial}{\partial x_i}\left(D_{3ij}\frac{\partial c_3}{\partial x_j}\right) - v_{3i}\frac{\partial c_3}{\partial x_i} = \frac{\partial c_3}{\partial t} + \frac{\xi_{31}}{n_3}(c_3 - c_1) + \frac{\xi_{32}}{n_3}(c_3 - c_2) \tag{3}$$

where subscripts 1, 2 and 3 represent macro-, meso- and micro-pores, respectively; subscripts i and j are coordinate indices, c is the solute concentration, t is the time after inception of the transport, x_i is the coordinate, D_{ij} is the hydrodynamic dispersion tensor, v_i is the average flow velocity, n is the porosity, and ξ is a concentration exchange coefficient characterizing the mass transfer among the pores of various scales.

A first approximation can be made by considering that: (a) the solute exchange between macropores and micropores is rather indirect and insignificant; (b) the mechani-

cal dispersion is prominent in macropores; (c) the convection is dominant in mesopores (McKibbin, 1985; Houseworth, 1988; Bouhroum, 1993); and, (d) the diffusion or replenishment is pervasive in micropores, as depicted in Fig. 1. As a result, Eq. (1)–(3) can be simplified as:

$$\frac{\partial}{\partial x_i}\left(D_{1ij}^{m}\frac{\partial c_1}{\partial x_j}\right) - v_{1i}\frac{\partial c_1}{\partial x_i} = \frac{\partial c_1}{\partial t} + \frac{\xi_{12}}{n_1}(c_1 - c_2) \tag{4}$$

$$-v_{2i}\frac{\partial c_2}{\partial x_i} = \frac{\partial c_2}{\partial t} + \frac{\xi_{21}}{n_2}(c_2 - c_1) + \frac{\xi_{23}}{n_2}(c_2 - c_3) \tag{5}$$

$$\frac{\partial}{\partial x_i}\left(D_{3ij}^{d}\frac{\partial c_3}{\partial x_j}\right) = \frac{\partial c_3}{\partial t} + \frac{\xi_{32}}{n_3}(c_3 - c_2) \tag{6}$$

where D_1^m is the mechanical dispersion coefficient, D_3^d is the effective diffusion coefficient incorporating the factor of tortuosity.

Further approximations can be made by assuming: (a) one-dimensional transport; (b) constant dispersivity and diffusivity; and, (c) spherical block structure of micropore aggregate (Huyakorn et al., 1983; Correa et al., 1987). As shown in Fig. 2, this spherical block represents an equivalent micropore domain with the outer bounding surface being defined as the mesopore skin. After dropping the superscripts for D_1 and D_3, Eq. (4), (5) and (6) can be modified as:

$$D_1\frac{\partial^2 c_1}{\partial x^2} - v_1\frac{\partial c_1}{\partial x} = \frac{\partial c_1}{\partial t} + \frac{\xi_{12}}{n_1}(c_1 - c_2) \tag{7}$$

$$-v_2\frac{\partial c_2}{\partial x} = \frac{\partial c_2}{\partial t} + \frac{\xi_{21}}{n_2}(c_2 - c_1) + \frac{3n_3D_3}{n_2R}\left[\frac{\partial c_3}{\partial r}\right]_{r=R} \tag{8}$$

$$\frac{D_3}{r^2}\frac{\partial}{\partial r}\left(r^2\frac{\partial c_3}{\partial r}\right) = \frac{\partial c_3}{\partial t} \tag{9}$$

where r is the radial distance from the center and R is the radius of the equivalent spherical micropore block, respectively. It may be noted from Eq. (9) that the transport in micropores is decoupled from that in mesopores. However, the coupling is restored in

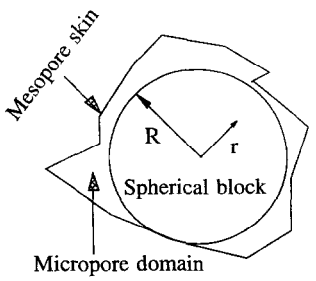

Fig. 2. Spherical block structure for micropores.

Eq. (8) by placing the flow in micropores as internal sources (sinks) for mesopores.

For more general solutions, the following dimensionless terms are introduced:

$$\begin{cases} y = \dfrac{x}{L}, \tau = \dfrac{v_1 t}{L}, \gamma_1 = \dfrac{v_1 L}{D_1}, \gamma_3^* = \dfrac{v_1 L}{D_3}, z = \dfrac{r}{L} \\ a_{ij} = \dfrac{\xi_{ij} L}{n_i v_i}, a^* = \dfrac{3 n_3 D_3}{n_2 R v_2}, b_i = \dfrac{v_1}{v_i}, R^* = \dfrac{r}{L} \end{cases} \tag{10}$$

where subscripts i and $j = 1, 2$; but $j \neq i$; L is an arbitrary length which may represent the length of testing core sample or the distance of pollutant migration from the source.

Incorporating all dimensionless terms, Eq. (7), (8) and (9) are rewritten as:

$$\frac{1}{\gamma_1}\frac{\partial^2 c_1}{\partial y^2} - \frac{\partial c_1}{\partial y} = b_1 \frac{\partial c_1}{\partial \tau} + a_{12}(c_1 - c_2) \tag{11}$$

$$-\frac{\partial c_2}{\partial y} = b_2 \frac{\partial c_2}{\partial \tau} + a_{21}(c_2 - c_1) + a^* \left[\frac{\partial c_3}{\partial z}\right]_{z=R/L} \tag{12}$$

$$\frac{1}{\gamma_3^*}\left(\frac{\partial^2 c_3}{\partial z^2} + \frac{2}{z}\frac{\partial c_3}{\partial z}\right) = \frac{\partial c_3}{\partial \tau} \tag{13}$$

For the step injection at the inlet and constant flux (zero flux for this case) at the outlet, boundary and initial conditions may be described by:

$$\begin{cases} c_1 = c_2 = c^0 & (y = 0) \\ \dfrac{\partial c_1}{\partial y} = 0 & (y = 1) \\ c_3 = \text{finite} & (z = 0) \\ c_3 = c_2 & (z = R/L) \\ c_1 = c_1^0\ c_2 = c_2^0\ c_3 = c_3^0 & (\tau = 0) \end{cases} \tag{14}$$

where c^0 is the concentration at the source, c_1^0, c_2^0 and c_3^0 are the initial concentrations in macropores, mesopores and micropores, respectively. The boundary conditions expounded in the above equations are applicable to the injected solute transport through a finite core column made up from a triple-porosity medium, as described in Fig. 3.

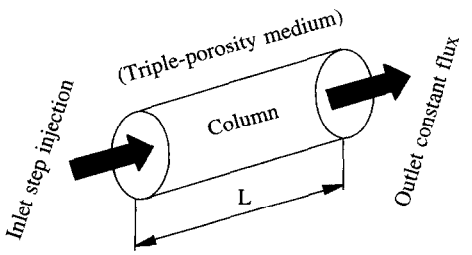

Fig. 3. Column injection for a triple-porosity medium.

Applying Laplace transform to Eq. (11), (12) and (13), one has:

$$\frac{1}{\gamma_1}\frac{d^2\bar{c}_1}{dy^2} - \frac{d\bar{c}_1}{dy} = b_1\left(s\bar{c}_1 - c_1^0\right) + a_{12}\left(\bar{c}_1 - \bar{c}_2\right) \tag{15}$$

$$-\frac{d\bar{c}_2}{dy} = b_2\left(s\bar{c}_2 - c_2^0\right) + a_{21}\left(\bar{c}_2 - \bar{c}_1\right) + a^*\left[\frac{d\bar{c}_3}{dz}\right]_{z=R/L} \tag{16}$$

$$\frac{1}{\gamma_3^*}\left(\frac{d^2\bar{c}_3}{dz^2} + \frac{2}{z}\frac{d\bar{c}_3}{dz}\right) = s\bar{c}_3 - c_3^0 \tag{17}$$

where s is a parameter in Laplace transform.

Boundary conditions in Laplace domain are changed to:

$$\begin{cases} \bar{c}_1 = \bar{c}_2 = \dfrac{c^0}{s} & (y=0) \\ \dfrac{d\bar{c}_1}{dy} = 0 & (y=1) \\ \bar{c}_3 = \text{finite} & (z=0) \\ \bar{c}_3 = \bar{c}_2 & (z=R/L) \end{cases} \tag{18}$$

$\bar{c}_3$ can be derived independently from Eq. (17). Following a similar procedure proposed by Moench (1984), one has:

$$\left[\frac{d\bar{c}_3}{dz}\right]_{z=R/L} = \left(\bar{c}_2 - \frac{c_3^0}{s}\right)\left[\phi\coth(\phi R/L) - \frac{L}{R}\right] \tag{19}$$

where $\phi = \sqrt{\gamma_3^* s}$.

Substituting Eq. (19) into Eq. (16), then:

$$-\frac{d\bar{c}_2}{dy} = (b_2 s + a_{21} + \psi_1)\bar{c}_2 - a_{21}\bar{c}_1 + \psi_1\psi_2 - b_2 c_2^0 \tag{20}$$

where,

$$\begin{cases} \psi_1 = a^*\left[\phi\coth(\phi R/L) - \dfrac{L}{R}\right] \\ \psi_2 = -\dfrac{c_3^0}{s} \end{cases} \tag{21}$$

Eq. (15) can be rewritten as:

$$\frac{1}{\gamma_1}\frac{d^2\bar{c}_1}{dy^2} - \frac{d\bar{c}_1}{dy} = (b_1 s + a_{12})\bar{c}_1 - a_{12}\bar{c}_2 - b_1 c_1^0 \tag{22}$$

The coupled Eq. (20) and (22) can be solved using the method of differential operators defined as:

$$D^{\bar{n}} f(x_i) = \frac{d^{\bar{n}} f(x_i)}{dx_i^{\bar{n}}} \tag{23}$$

where i indexes an arbitrary variable, and $\bar{n}$ is the order of the differential equations.

Applying the differential operator, Eq. (20) and (22) become:

$$(D + \psi_4)\bar{c}_2 - a_{21}\bar{c}_1 = -\psi_5 \tag{24}$$

$$\left[\frac{1}{\gamma_1} D^2 - D - \psi_3\right]\bar{c}_1 + a_{12}\bar{c}_2 = -b_1 c_1^0 \tag{25}$$

where,

$$\begin{cases} \psi_3 = b_1 s + a_{12} \\ \psi_4 = b_2 s + a_{21} + \psi_1 \\ \psi_5 = \psi_1 \psi_2 - b_2 c_2^0 \end{cases} \tag{26}$$

Eq. (24) can be reformulated as:

$$\bar{c}_1 = \frac{1}{a_{21}}\left[(D + \psi_4)\bar{c}_2 + \psi_5\right] \tag{27}$$

Substituting Eq. (27) into Eq. (25), yields:

$$D^* \bar{c}_2 = \theta_4 \tag{28}$$

where,

$$\begin{cases} D^* = D^3 + \theta_1 D^2 + \theta_2 D + \theta_3 \\ \theta_1 = \psi_4 - \gamma_1 \\ \theta_2 = -\gamma_1(\psi_3 + \psi_4) \\ \theta_3 = \gamma_1(a_{12} a_{21} - \psi_3 \psi_4) \\ \theta_4 = \gamma_1(\psi_3 \psi_5 - a_{21} b_1 c_1^0) \end{cases} \tag{29}$$

The solution $\bar{c}_2$ of Eq. (28) can be expressed as:

$$\bar{c}_2 = \bar{c}_2^h + \bar{c}_2^n \tag{30}$$

where $\bar{c}_2^h$ and $\bar{c}_2^n$ are the homogeneous and nonhomogeneous solutions, respectively; where $\bar{c}_2^n$ can be derived as:

$$\bar{c}_2^n = \theta_3^{-1}\theta_4 \tag{31}$$

For homogeneous solutions $\bar{c}_2^h$, the roots of D^* in Eq. (28) can be derived as follows. Let:

$$D_i = Z_i - \frac{\theta_1}{3} \tag{32}$$

where $i = 1$, 2, and 3.

Substituting Eq. (32) into Eq. (28) gives:

$$Z^3 + pZ + q = 0 \tag{33}$$

where,

$$\begin{cases} p = \theta_2 - \dfrac{\theta_1^2}{3} \\ q = \dfrac{2}{27}\theta_1^3 - \dfrac{\theta_1\theta_2}{3} + \theta_3 \end{cases} \tag{34}$$

Three roots of Eq. (33) may be described as follows:

$$\begin{cases} Z_1 = B_1 + B_2 \\ Z_2 = \omega_1 B_1 + \omega_2 B_2 \\ Z_3 = \omega_2 B_1 + \omega_1 B_2 \end{cases} \tag{35}$$

where,

$$\begin{cases} \Delta = \left(\dfrac{q}{2}\right)^2 + \left(\dfrac{p}{3}\right)^3 \\ B_1 = \left\{-\dfrac{q}{2} + \sqrt{\Delta}\right\}^{\frac{1}{3}}, \quad B_2 = \left\{-\dfrac{q}{2} - \sqrt{\Delta}\right\}^{\frac{1}{3}} \\ \omega_1 = -\dfrac{1}{2} + \dfrac{\sqrt{3}}{2}i, \quad \omega_2 = -\dfrac{1}{2} - \dfrac{\sqrt{3}}{2}i \end{cases} \tag{36}$$

As a result, the roots of D^* in Eq. (28) can be derived. Because Δ in Eq. (36) may have three different signs, the solutions should be expressed individually. For briefness, the detailed derivation of $\bar{c}_1$ and $\bar{c}_2$ in accordance is given in the Appendix.

After deriving $\bar{c}_2$ from Eq. (28), $\bar{c}_1$ can be obtained by substituting $\bar{c}_2$ into Eq. (27). The solute concentrations in the original space for macropores c_1 and for mesopores c_2 can be obtained through numerical inversion (Stehfest, 1970).

4. Parametric study

Field observations appear to support the existence of the triple-porosity transport phenomenon. Measurements on a forested watershed in eastern Tennessee revealed that about 70% of ponded infiltration was transported by a pore region with pore diameter greater than 1 mm, or the macropores, and about 20% of the flux was transported by a pore region with EPD between 1 mm and 0.005 mm, or mesopores (Watson and Luxmoore, 1986). Micropores with EPD smaller than 0.01 mm may occupy a relatively large space but contribute indirectly to the regional flow through predominant diffusive process. While the availability of field data for the triple-porosity media may be rather restricted (Gwo et al., 1995), the derivable parameters for the dual-porosity media and the proposed experimental procedures to determine these parameters can be referred to Berryman and Wang (1995).

Table 1
Selected dimensionless parameters

Figure	γ_1	γ_3	a^*	a_{12}	a_{21}	b_1	b_2	R^*	c_1^0	c_2^0	c_3^0	τ	y
4	1–100	10	100	0.5	1	1	2	10^{-5}	0.001	0.002	0.003	0.8	0–1
5	1	10	100–5000	0.5	1	1	2	10^{-5}	0.001	0.002	0.003	0.8	0–1
6	1	10	100	0.1–1	1	1	2	10^{-5}	0.001	0.002	0.003	0.8	0–1
7	1	10	100	0.5	5	1	2–10	10^{-5}	0.001	0.002	0.003	0.8	0–1
8	1	10	5000	1	1	1	2	10^{-5}	0.001	0.002	0.003	0.8	0–1
9	1–100	10	100	0.5	1	1	2	10^{-5}	0.001	0.002	0.003	0–3	0.75
10	1	10	100	0.5	1	1	2–5	10^{-5}	0.001	0.002	0.003	0–3	0.75
11	1	10	5000	1	1	1	2	10^{-5}	0.001	0.002	0.003	0–3	0.75

Because the comprehensive probe on the experimental determination of triple-porosity parameters is beyond the scope of the present analysis, the parametric study focuses merely on the sensitivity analysis of certain critical parameters. The primary dimensionless parameters in the present model are the equivalent quantities of: (a) Peclet number (EPN) γ, (b) micropore source (sink) strength a^*, (c) solute exchange coefficient a_{12} and a_{21}, and (d) velocity ratio b. Selected parameters are listed in Table 1 with associated figures. The selection of some parameters is based on the certain physical intuition such as $b_1 < b_2$ owing to $v_1 > v_2$. Other selections show uncertain relationship because multiple parameters are involved (e.g., γ_i and a_{ij}). The illustrated relative concentration c/c_0 is referred to macropores c_1 where primary flow pathways are imbedded. The dimensionless time is referred to τ, or injected pore volume. For comparison, single- and dual-porosity models are readily derived from the present triple-porosity model by independently assuming a_{12} or a^* to be zero, respectively.

It should be noted that the designation of γ_3^* does not reflect the influence of macropore velocity on the micropore transport because the velocity terms are canceled out naturally in the micropore equation. The selection of EPN for macropore γ_1 and for micropore γ_3^* is rather arbitrary. If assuming that the diffusion coefficient D_3 is smaller than dispersion coefficient D_1, then γ_1 is in general less than γ_3^*. Fig. 4 depicts the spatial concentration distribution subject to the variations of the EPN in the macropores γ_1. Except at the down stream, larger γ_1 appears to be related to the solute transport at more restricted regions near the source. In any case, dramatic changes in γ_1 result in less substantial solute variations.

Because the interporosity mass transport is determined by the relative concentration difference between various pore spaces, this process can exert significant impact on the fate of contaminant migration. As described by the governing equations, the internal solute exchange can be considered either as sources or sinks, depending on the signs of the concentration differences. Fig. 5 shows the spatial variations of solute concentration as a result of the change in micropore source (sink) strength a^*. This term alone sets a distinction between a dual-porosity model and a triple-porosity one. It is apparent that the increased mass transfer between micro- and mesopores would promote a farther solute spreading to a more remote location, in particular at down stream.

Solute interporosity exchange can be further examined by envisioning the transport process between meso- and macropores, as reflected by the magnitude of the equivalent

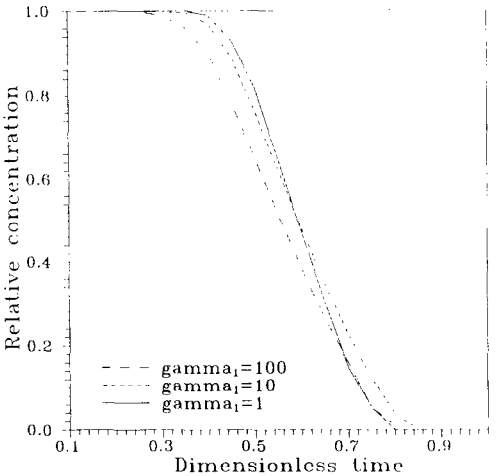

Fig. 4. Spatial concentration for various γ_1.

exchange coefficients a_{12} and a_{21}. It should be noted that a_{12} may not be equal to a_{21} since they consist of different porosity and velocity terms, even though $\xi_{12} = \xi_{21}$. This uncertainty is due to the paradoxical relationship between the products of porosity n and velocity v, for which $v_1 > v_2$ and $n_2 > n_1$ in general. This relationship is examined in Fig. 6. It appears that the greater exchange between two larger porous spaces leads to a more extensive solute migration.

For more dramatic comparison, a_{21} is deliberately enlarged to decrease the effect of mesopore storativity. As expected, velocity contrasts between two primary pore spaces (i.e. macro- and mesopores) seem to exert a significant impact in solute transport

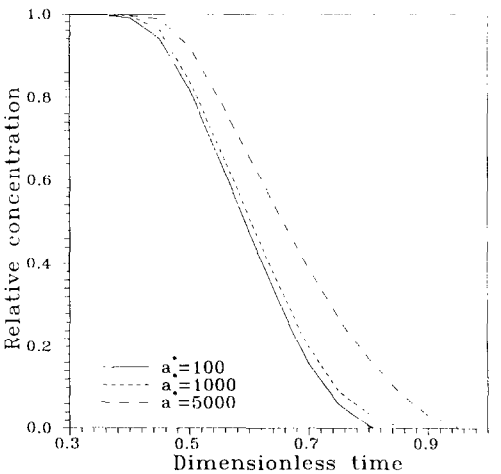

Fig. 5. Spatial concentration for various a^*.

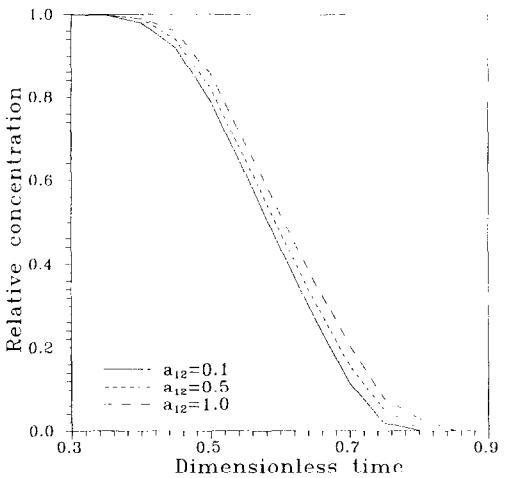

Fig. 6. Spatial concentration for various a_{ij}.

(Bouhroum, 1993). Because b_2 indexes the velocity ratio between macro- and mesopores, an increase of b_2, as depicted in Fig. 7, indicates a magnification of velocity contrast between the two domains. It is of interest to observe that, as b_2 increases, a dispersion dominant phenomenon is transforming to a convection dominant process with the increased sharp concentration front. More interestingly, variations of concentration slopes are readily observed at the upper stream when $b_2 = 3$ and $b_2 = 4$. This is an indication of mass transfer to the primary flow channels from the less permeable regions when the stored mass within the channels become exhausted. The behavior of variable

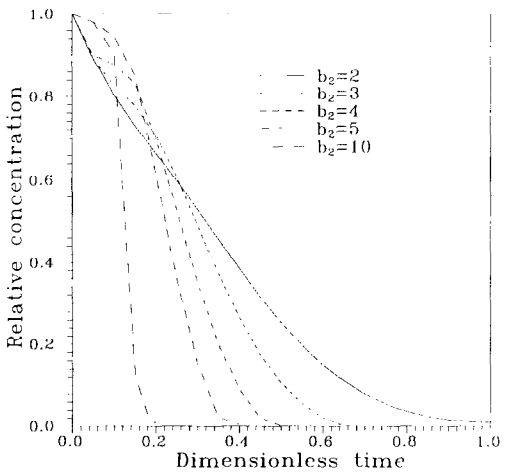

Fig. 7. Spatial concentration for various b_i.

concentration changes was frequently recorded in the experiments (Neretnieks, 1993; Bai and Roegiers, 1995).

Comparisons between the present triple-porosity model with traditional single- and dual-porosity models are desirable as a means to demonstrate the flexibility of using a higher porosity modeling approach. Owing to the difficulties associated with maintaining compatible parameters and boundary as well as initial conditions between various models of similar conceptualizations, both single- and dual-porosity models are derived from the present triple-porosity model by independently assuming $a_{12} = 0$ for the former and $a^* = 0$ for the latter case, respectively. Furthermore, both a^* and a_{12} are adjusted to achieve more significant results. The subsequent comparison is shown in Fig. 8. The spatial concentration for the triple-porosity model appears to fall within those of other two models, with slight bias towards the single-porosity model. In other words, the effect of traditional dual-porosity phenomenon between macro- and micropores may have been mitigated due to the existence of a buffer zone, mesopores, under present circumstance.

Related to the possibility of field measurements, it would be of interest to analyze the temporal solute transport at the designated location in triple-porosity media. Fig. 9 depicts the breakthrough curves under the variation of the EPN in macropores. It appears that the larger EPNs tend to prolong the concentration variations with extended tailing, which is in clear contrast to more rapid and abrupt concentration changes with shorter tails when EPNs become relatively small. In addition to either dispersion or convection dominant mechanisms related to either former (smaller γ_1) or latter (larger γ_1) behaviors, the added abnormality seems to be associated with the interactive multi-porosity processes.

The increase of velocity ratio b, even though in relatively narrow ranges, results in substantial time lags of breakthrough curves, as shown in Fig. 10. Larger velocity contrasts between macropores and mesopores generally lead to much delayed break-

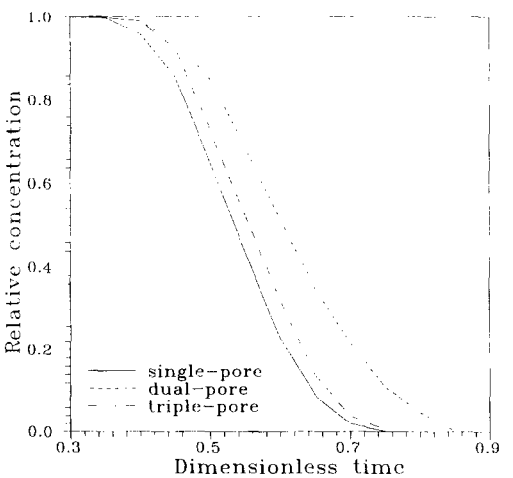

Fig. 8. Spatial comparison for various models.

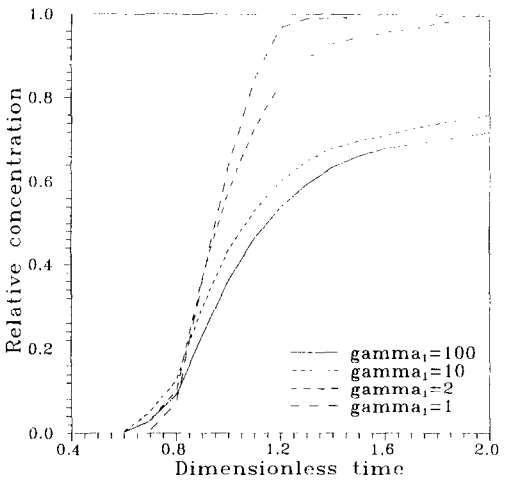

Fig. 9. Temporal concentration for various γ_1.

through, as a result of increasing mass exchange between the two interacting porous spaces.

Temporal comparisons of solute concentration between single-, dual- and triple-porosity models are illustrated in Fig. 11. Contrary to the spatial comparison shown in Fig. 8, the temporal concentration change for the triple-porosity model represents the earliest breakthrough, as opposite to the latest breakthrough for the dual-porosity model. Under this situation, the mesopores promote the solute breakthrough by assisting the mass supply to the primary flow channels from the less permeable micropores. In

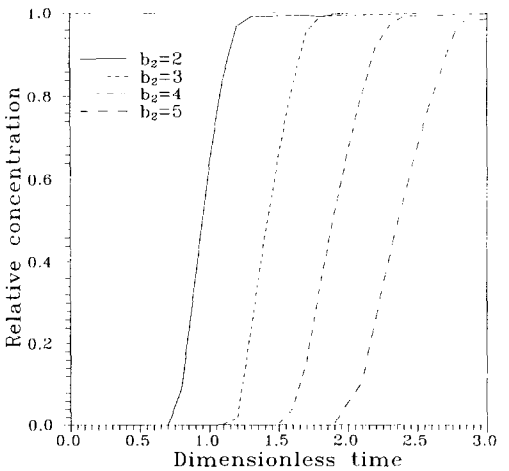

Fig. 10. Temporal concentration for various b_i.

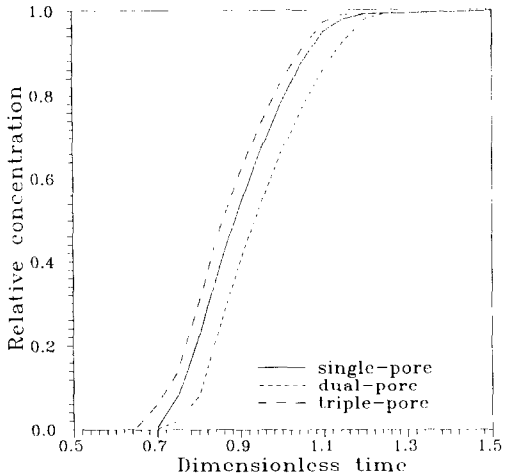

Fig. 11. Temporal comparison for various models.

comparison, convective transport in mesopores for the triple-porosity media may overshadow the diffusive process within the micropores.

5. Conclusions

Based on the multiporosity/multipermeability concept introduced by Bai et al. (1993), a triple-porosity model has been presented to study the contaminant transport in heterogeneous porous media. With reference to the conductance and storage characteristics in each pore domain, this triple-porosity structure comprises: (a) macropores as primary flow paths where both dispersion and convection are prevalent; (b) mesopores as intermediate flow paths where convection becomes dominant; and (c) micropores as supplemental flow paths and mass storage spaces where only diffusive flow is manifest.

Partial decoupling of flow between micropores and mesopores is obtained by assuming a purely diffusive flow within the former space. The coupling, however, is restored by placing the micropore diffusion as internal sources (sinks) attached to mesopore skins. Full coupling is maintained between macropores and mesopores. The coupled equations are circumvented via the method of differential operators to enable the semi-analytical solutions to be derived in a one-dimensional transport geometry.

Parametric study identifies the significant influential factors such as the ratio of flow velocity and the equivalent Peclet number. In comparison with traditional single- and dual-porosity models, the presented triple-porosity model may offer an efficient means to validate existing numerical models for similar complex systems and may provide additional flexibility in matching pertinent experimental data.

Acknowledgements

Support of the National Science Foundation, Oklahoma State and industrial consortium under contract EEC-9209619 is gratefully acknowledged. M. Bai would like to

express his appreciation to Drs. D. Elsworth, A. Bouhroum and F. Civan for their useful comments and technical assistance.

Appendix A. Derivation of $\bar{c}_1$ and $\bar{c}_2$

A.1. Solutions when $\Delta > 0$

Solutions of D^* yield one real and two complex roots:

$$\begin{cases} D_1 = B_1 + B_2 - \dfrac{\theta_1}{3} \\ D_2 = -\dfrac{1}{2}(B_1 + B_2) + \dfrac{\sqrt{3}}{2}(B_1 - B_2)i - \dfrac{\theta_1}{3} \\ D_3 = -\dfrac{1}{2}(B_1 + B_2) - \dfrac{\sqrt{3}}{2}(B_1 - B_2)i - \dfrac{\theta_1}{3} \end{cases} \tag{A1}$$

The solution for $\bar{c}_1$ can be given as:

$$\bar{c}_1 = \frac{1}{a_{21}}(E_1 + E_2 + E_3 + E_4) \tag{A2}$$

where:

$$\begin{cases} E_1 = e_1 e^{\xi_1 y}(\xi_1 + \psi_4) \\ E_2 = e_2 e^{\xi_2 y}[(\psi_4 - \xi_2)\cos(\xi_3 y) - \xi_3 \sin(\xi_3 y)] \\ E_3 = e_3 e^{-\xi_2 y}[(\psi_4 - \xi_2)\sin(\xi_3 y) + \xi_3 \cos(\xi_3 y)] \\ E_4 = \theta_3^{-1}\theta_4\psi_4 + \psi_5 \end{cases} \tag{A3}$$

where: e_1, e_2 and e_3 are constants to be determined through satisfying boundary conditions; and

$$\begin{cases} \xi_1 = B_1 + B_2 - \dfrac{\theta_1}{3} \\ \xi_2 = \dfrac{1}{2}(B_1 + B_2) + \dfrac{\theta_1}{3} \\ \xi_3 = \dfrac{\sqrt{3}}{2}(B_1 - B_2) \end{cases} \tag{A4}$$

Similarly, $\bar{c}_2$ can be expressed as:

$$\bar{c}_2 = e_1 e^{\xi_1 y} + e_2 e^{-\xi_2 y}\cos(\xi_3 y) + e_3 e^{-\xi_2 y}\sin(\xi_3 y) + \theta_3^{-1}\theta_4 \tag{A5}$$

Assuming:

$$\begin{cases} \beta_1 = \xi_1 + \psi_4, \quad \beta_2 = \psi_4 - \xi_2 \\ \beta_3 = \dfrac{c^0}{s} - \theta_3^{-1}\theta_4 \quad \beta_4 = \xi_1 e^{\xi_1}\beta_1 \\ \beta_5 = e^{-\xi_2}\{\xi_3(2\xi_2 - \psi_4)\sin(\xi_3) - [\xi_3^2 + \xi_2(\psi_4 - \xi_2)]\cos(\xi_3)\} \\ \beta_6 = e^{-\xi_2}\{[\xi_2(\psi_4 - \xi_2) - \xi_3^2]\sin(\xi_3) + \xi_3(\psi_4 - 2\xi_2)\cos(\xi_3)\} \\ \beta_7 = \dfrac{c^0}{s}a_{21} - (\theta_3^{-1}\theta_4\psi_4 + \psi_5) \end{cases} \tag{A6}$$

After satisfying the boundary conditions of Eq. (18), e_1, e_2 and e_3 are derived as given in the following equations:

$$e_1 = \frac{W_1}{M}, \quad e_2 = \frac{W_2}{M}, \quad e_3 = \frac{W_3}{M} \tag{A7}$$

where:

$$\begin{cases} M = \beta_6(\beta_2 - \beta_1) + \xi_3(\beta_4 - \beta_5) \\ W_1 = \beta_3(\beta_2\beta_6 - \xi_3\beta_5) - \beta_7\beta_6 \\ W_2 = \beta_7\beta_6 - \beta_3(\beta_1\beta_6 - \xi_3\beta_4) \\ W_3 = \beta_7(\beta_4 - \beta_5) + \beta_3(\beta_1\beta_5 - \beta_2\beta_4) \end{cases} \tag{A8}$$

A.2. Solutions when $\Delta = 0$

Solutions of D^* have three real roots. The solutions of $\bar{c}_1$ and $\bar{c}_2$ can be simply expressed as follows:

$$\bar{c}_1 = \frac{1}{a_{21}}\{e_1 e^{-\eta_1 y}(\psi_4 - \eta_1) + e_2 e^{-\eta_2 y}(\psi_4 - \eta_2) + e_3 e^{-\eta_2 y}[1 + y(\psi_4 - \eta_2)] + \psi_4\theta_3^{-1}\theta_4 + \psi_5\} \tag{A9}$$

$$\bar{c}_2 = e_1 e^{-\eta_1 y} + e_2 e^{-\eta_2 y} + e_3 y e^{-\eta_2 y} + \theta_3^{-1}\theta_4 \tag{A10}$$

where:

$$\begin{cases} \eta_1 = \sqrt[3]{4q} + \dfrac{\theta_1}{3} \\ \eta_2 = \eta_3 = \sqrt[3]{\dfrac{q}{2}} + \dfrac{\theta_1}{3} \end{cases} \tag{A11}$$

Let:

$$\begin{cases} \delta_1 = \psi_4 - \eta_1, \quad \delta_2 = \psi_4 - \eta_2 \\ \delta_3 = -\eta_1 e^{-\eta_1}\delta_1, \quad \delta_4 = -\eta_2 e^{-\eta_2}\delta_2 \\ \delta_5 = \left[\psi_4 - \eta_2(2 + \psi_4 - \eta_2)\right] e^{-\eta_2} \end{cases} \tag{A12}$$

The constants e_1, e_2 and e_3 given in Eq. (A9) and (A10) have identical forms as in Eq. (A7) but are expressed by the following M, W_1, W_2 and W_3:

$$\begin{cases} M = \delta_5(\delta_2 - \delta_1) + \delta_3 - \delta_4 \\ W_1 = \beta_3(\delta_2\delta_5 - \delta_4) - \beta_7\delta_5 \\ W_2 = \beta_7\delta_5 - \beta_3(\delta_1\delta_5 - \delta_3) \\ W_3 = \beta_7(\delta_3 - \delta_4) + \beta_3(\delta_1\delta_4 - \delta_2\delta_3) \end{cases} \tag{A13}$$

A.3. Solutions when $\Delta < 0$

Solutions of D^* have three different real roots. The roots of D^* in trigonometric expression is given as:

$$\begin{cases} \rho_1 = 2\sqrt[3]{r^*}\cos\left(\dfrac{\alpha}{3}\right) - \dfrac{\theta_1}{3} \\ \rho_2 = 2\sqrt[3]{r^*}\cos\left(\dfrac{\alpha}{3} + 120°\right) - \dfrac{\theta_1}{3} \\ \rho_3 = 2\sqrt[3]{r^*}\cos\left(\dfrac{\alpha}{3} + 240°\right) - \dfrac{\theta_1}{3} \end{cases} \tag{A14}$$

where:

$$\begin{cases} r^* = \sqrt{-\left(\dfrac{p}{3}\right)^3} \\ \alpha = \arccos\left(-\dfrac{q}{2r^*}\right) \end{cases} \tag{A15}$$

The solutions of $\bar{c}_1$ and $\bar{c}_2$ are described as follows:

$$\bar{c}_1 = \frac{1}{a_{21}}\left\{e_1 e^{\rho_1 y}(\rho_1 + \psi_4) + e_2 e^{\rho_2 y}(\rho_2 + \psi_4) + e_3 e^{\rho_3 y}(\rho_3 + \psi_4) + \psi_4\theta_3^{-1}\theta_4 + \psi_5\right\} \tag{A16}$$

$$\bar{c}_2 = e_1 e^{\rho_1 y} + e_2 e^{\rho_2 y} + e_3 e^{\rho_3 y} + \theta_3^{-1}\theta_4 \tag{A17}$$

Let:

$$\begin{cases} \sigma_1 = \rho_1 + \psi_4, \quad \sigma_2 = \rho_2 + \psi_4, \quad \sigma_3 = \rho_3 + \psi_4 \\ \sigma_4 = \rho_1 e^{\rho_1}\sigma_1, \quad \sigma_5 = \rho_2 e^{\rho_2}\sigma_2, \quad \sigma_6 = \rho_3 e^{\rho_3}\sigma_3 \end{cases} \tag{A18}$$

Similarly, the constants e_1, e_2 and e_3 given in Eq. (A16) and (A17) have identical forms as in Eq. (A7) but are expressed by the following M, W_1, W_2 and W_3:

$$\begin{cases} M = \sigma_6(\sigma_2 - \sigma_1) + \sigma_5(\sigma_1 - \sigma_3) + \sigma_4(\sigma_3 - \sigma_2) \\ W_1 = \beta_3(\sigma_2\sigma_6 - \sigma_3\sigma_5) + \beta_7(\sigma_5 - \sigma_6) \\ W_2 = \beta_7(\sigma_6 - \sigma_4) - \beta_3(\sigma_1\sigma_6 - \sigma_3\sigma_4) \\ W_3 = \beta_7(\sigma_4 - \sigma_5) + \beta_3(\sigma_1\sigma_5 - \sigma_2\sigma_4) \end{cases} \tag{A19}$$

The solute concentrations in real space c_1, c_2 and c_3 can be obtained by invoking a numerical inversion technique (Stehfest, 1970).

References

Bai, M. and Elsworth, D., 1995. On the modeling of miscible flow in multi-component porous media. J. Transport in Porous Media, 21: 19–46.

Bai, M., Elsworth, D. and Roegiers, J.-C., 1993. Multi-porosity/multi-permeability approach to the simulation of naturally fractured reservoirs. Water Resour. Res., 29(6): 1621–1633.

Bai, M. and Roegiers, J.-C., 1994. On the correlation of nonlinear flow and linear transport with application to dual-porosity modeling. J. Petroleum Sci. and Engng., 11: 63–72.

Bai, M. and Roegiers, J.-C., 1995. Modeling of heat flow and solute transport in fractured rock masses. Proc. 8th Int. Congress on Rock Mech., Japan, pp. 787–793.

Bear, J., 1972. Dynamics of Fluids in Porous Media. Elsevier, New York.

Bear, J., 1993. Modeling flow and contaminant transport in fractured rock. In: J. Bear, C.-F. Tsang and G. De Marsily (Editors). Flow and Contaminant Transport in Fractured Rock. Academic Press, San Diego, CA, pp. 1–37.

Berryman, J.G. and Wang, H.F., 1995. The elastic coefficients of double-porosity models for fluid transport in jointed rock. J. Geophys. Res., 100: B12, 24611–24627.

Bibby, R., 1981. Mass transport of solutes in dual-porosity media. Water Resour. Res., 17: 1075–1081.

Bouhroum, A., 1993. Is tailing of breakthrough curves diffusive? Theoretical and experimental evaluation, paper 13, 5th Saskatchewan Petroleum Conf., Regina, Canada.

Bouhroum, A. and Bai, M., 1996. Experimental and numerical simulation of solute transport in heterogeneous porous media. Int. J. Num. Analy. Meth. Geomech., 20: 155–171.

Correa, A.C., Pande, K.K. and Ramey, H.J., 1987. Prediction and interpretation of miscible displacement performance using a transverse matrix dispersion model, SPE 16756, 62nd Annual Tech. Conf. and Exhib., Dallas,

Coats, K.H. and Smith, B.D., 1964. Dead-end pore volume and dispersion in porous media. SPEJ, 4: 73–84.

Gwo, J.P., Jardine, P.M., Wilson, G.V. and Yeh, G.T., 1995. A multiple-pore-region concept to modeling mass transfer in subsurface media. J. Hydrology, 164: 217–237.

Harrison, B., Sudicky, E.A. and Cherry, J.A., 1992. Numerical analysis of solute migration through fractured clayey deposits into underlying aquifers. Water Resour. Res., 28: 515–526.

Houseworth, J.E., 1988. Characterizing permeability heterogeneity in core samples from standard miscible displacement experiments, SPE 18329, 63rd SPE Annual Tech. Conf. and Exhib., Houston, TX, 12 pp.

Huyakorn, P.S., Lester, B.H. and Faust, C.R., 1983. Finite element techniques for modeling groundwater flow in fractured aquifers. Water Resour. Res., 19: 1019-1035.

Imdakm, A.O. and Sahimi, M., 1991. Computer simulation of particle transport processes in flow through porous media. Chem. Eng., 46: 1977–1993.

Joy, D.M. and Kouwen, N., 1991. Particulate transport in a porous medium under non-linear flow conditions. J. Hydraulic Res., 29: 373–385.

Joy, D.M., Lennox, W.C. and Kouwen, N., 1993. Stochastic model of particulate transport. J. Hydraulic Eng., 119: 846–861.

Koenders, M.A. and Williams, A.F., 1992. Flow equations of particle fluid mixtures. Acta Mechanica, 92: 91–116.

Leo, C.J. and Booker, J.R., 1993. Boundary element analysis of contaminant transport in fractured porous media. Int. J. Numer. Analytic. Methods Geomech., 17: 471–492.

Luxmoore, R.J., Jardine, P.M., Wilson, G.V., Jones, J.R. and Zelazny, L.W., 1990. Physical and chemical controls of preferred path flow through a forest hillslope. Geoderma, 46: 139–154.

McKibbin, R., 1985. Thermal convection in layered and anisotropic porous media: a review. Proc. CSIRO/DSIR Seminar on Convective Flows in Porous Media, Wellington, New Zealand, pp. 113–127.

Moench, A.F., 1984. Double-porosity models for a fissured groundwater reservoir with fracture skin. Water Resour. Res., 20: 831–846.

Neretnieks, I., 1993. Solute transport in fractured rock—applications to radionuclide waste repositories. In: J. Bear, C.-F. Tsang and G. De Marsily (Editors). Flow and Contaminant Transport in Fractured Rock, Academic Press, San Diego, CA, pp. 39–128.

Nilson, R.H. and Lie, K.H., 1990. Double-porosity modeling of oscillatory gas motion and contaminant transport in a fractured porous medium. Int. J. Numer. Analytic. Methods Geomech., 14: 565–585.

Noltimier, H.C., 1971. A model for grain dispersion and magnetic anisotropy in sedimentary rocks. J. Geophy. Res., 76: 3990–4002.

Passioura, J.B., 1971. Hydrodynamic dispersion in aggregated media, 1. Theory. Soil Sci., 111: 339–344.

Passioura, J.B. and Rose, D.A., 1971. Hydrodynamic dispersion in aggregated media, 2. Effects of velocity and aggregate size. Soil Sci., 111: 345–351.

Piquemal, J., 1992. On the modeling of miscible displacements in porous media with stagnant fluid. Transport in Porous Media, 8: 243–262.

Piquemal, J., 1993. On the modeling conditions of miscible displacements in porous media presenting capacitance effects by a dispersion–convection equation for the mobile fluid and a diffusion equation for the stagnant fluid. Transport in Porous Media, 10: 271–283.

Rowe, R.K. and Booker, J.R., 1990. Contaminant migration in a regular two- or three-dimensional fractured network: reactive contaminants. Int. J. Numer. Analytic. Methods Geomech., 14: 401–425.

Sahimi, M., 1993. Flow phenomena in rocks: from continuum models to fractals, percolation, cellular automata, and simulated annealing. Rev. Mod. Phys., 65: 1393–1534.

Sardin, M., Schweich, D., Leij, F.J. and van Genuchten, M.T., 1991. Modeling the nonequilibrium transport of linearly interacting solutes in porous media: a review. Water Resour. Res., 27: 2287–2307.

Shackelford, C.D., 1993. Contaminant transport. In: D.E. Daniel (Editor). Geotechnical Practice for Waste Disposal. Chapman and Hall, London, pp. 33–65.

Stehfest, H., 1970. Algorithm 358—Numerical inversion of Laplace transforms. Communications of ACM, 13: 47–49.

Sudicky, E.A. and Mclaren, R.G., 1992. The Laplace transform Galerkin technique for large-scale simulation of mass transport in discretely fractured porous formations. Water Resour. Res., 28: 499–514.

Tang, D.H., Frind, E.O. and Sudicky, E.A., 1981. Contaminant transport in fractured porous media: analytical solution for a single fracture. Water Resour. Res., 17: 555–564.

Warren, J.E. and Root, P.J., 1963. Behavior of naturally fractured reservoirs. SPEJ., 228: 245–255.

Watson, K.W. and Luxmoore, R.J., 1986. Estimating macroporosity in a forest watershed by use of a tension infiltrometer. Soil Sci. Soc. Am. J., 50: 578–582.